Nanofibrous cobalt oxide for electrocatalysis of CO_2 reduction to carbon monoxide and formate in an acetonitrile-water electrolyte solution

Abdalaziz Aljabour[a,b,c,*], Halime Coskun[b], Dogukan Hazar Apaydin[b], Faruk Ozel[d], Achim Walter Hassel[c], Philipp Stadler[b], Niyazi Serdar Sariciftci[b], Mahmut Kus[a]

[a] Selcuk University, Department of Chemical Engineering, 42075, Konya, Turkey
[b] Linz Institute for Organic Solar Cells (LIOS), Physical Chemistry, Johannes Kepler University Linz, Altenberger Strasse 69, A-4040 Linz, Austria
[c] Institute for Chemical Technology of Inorganic Materials, Johannes Kepler University, Altenberger Straße 69, A-4040 Linz, Austria
[d] Karamanoglu Mehmetbey University, Department of Metallurgical and Materials Engineering, 70100, Karaman, Turkey

ABSTRACT

The electrocatalytic reduction of carbon dioxide (CO_2) is an attractive option to efficiently bind electrical energy from renewable resources in artificial carbon fuels and feedstocks. The strategy is considered as crucial part in closing the anthropogenic carbon cycle. In particular, the electrosynthetic production of C1 species such as carbon monoxide (CO) would radiate immense power, since these building blocks offer a versatile chemistry to higher carbon products and fuels. In the present study we report the exploration of the catalytic behavior of semiconducting Co_3O_4 nanofibers for the conversion of CO_2 to CO predominantly with a Faradaic efficiency of 65%. We assist the process by expanding the electrode network with nanofibrous interconnections and hence are able to demonstrate the electrosynthesis of CO without applying any metal supplement. We use polyacrylnitrile (PAN) as template polymer to generate highly crystalline Co_3O_4 fibers to expand the catalytically active surface to volume ratio. The stability of the nanofibrous electrodes remains for 8 h at a geometric current density of approximately 0.5 mA/cm^2 on a flat surface. The ease of synthesis and the comparatively high Faradaic yield for CO makes Co_3O_4 nanofibers a potential candidate for future large scale electrode utilization.

1. Introduction

The electrosynthetic recycling of CO_2 in carbon capture and utilization (CCU) is a growing field – anthropogenic emitted CO_2 can be used as future carbon feedstock for the conversion into useful chemical products and synthetic fuels using renewable, CO_2 free energy sources [1]. However, the electrochemical reduction of CO_2 requires a highly negative potential of -1.9 V versus standard hydrogen electrode (SHE) for one electron reduction [2].

In practice, these potentials are further increased due to overpotentials and kinetic barriers at the electrodes. To overcome these issues, powerful electrocatalysts are required which combine high Faradaic efficiencies and energy yields as well as high turnover. This can be realized by immobilized electrocatalysts which offer large effective surface areas [3–6].

In this work, we report that Co_3O_4 nanofibers work as CO_2 selective electrocatalyst on fluorine doped tin oxide (FTO) electrodes. A facile electrospinning technique allows the deposition of high catalytic activity Co_3O_4 networks. While numerous alternative activated cobalt

systems (plane Co, CoO, Co-organic complexes) have demonstrated the catalytic conversion of CO_2 into hydrocarbons, such as CH_4 and similar, CO production has been observed only in the presence of metal additives, in particular palladium, platinum, and/or alkali promoters like potassium [7]. In Table 1, the prior-art on cobalt catalysts in CO_2 reduction is provided.

Recently, Co_3O_4 thin films were applied in electrocatalytic formate formation from CO_2 [14], however to date pristine cobalt in CO production and thus the application of Co_3O_4 nanofibers in electrocatalysis has not been explored in detail yet. Although CO itself is another important feedstock with an extended field of application, low efficiency of CO production ($\sim$10%) is reported with the catalytically active cobalt intermixed with palladium and potassium [12]. Higher efficiency (60%) for CO evolution is only observed with complex organic cobalt compounds but with limited catalyst stability [11]. Therefore, the aim of this study is to use pristine Co_3O_4, synthesized through a facile synthesis route, in the conversion of CO_2 to CO. Any comparison in electrochemical behavior with other cobalt compounds, i.e. Co_3O_4 nanoparticles are not considered in this study due to the variation in the

Table 1
State-of-the-art on cobalt electrocatalysts in CO_2 reduction.

Catalyst	Electrolyte solution	Potential	CO [%]	HCOO$^-$ [%]	Stability	Ref.
Ag-Co bimetallic catalyst	1) 0.5 M $KHCO_3$ 1) $TBAPF_6$ in DMF	-2 V vs SHE	7.8	N.A.	N.A.	[8]
Molecular Co Complexes	0.1 M NBu_4BF_4 in DMF + various w% H_2O	-2 V vs $Fc^{+/0}$	< 1	90	~1 h	[9]
Co_3O_4 single-unit-cell layer	0.1 M $KHCO_3$	-0.87 V vs SCE	< 10	> 85	40 h	[10]
Cobalt protoporphyrin	0.1 M $HClO_4$	-0.6 V vs RHE	60	N.A.	1 h	[11]
Co + w% Pd + w% K	N.A.	N.A.	< 11	N.A.	N.A.	[12]
Atomic Cobalt layers	0.1 M Na_2SO_4	-0.85 V vs SCE	N.A.	~90	60 h	[13]
Ultrathin Co_3O_4	0.1 M $KHCO_3$	-0.88 V vs SCE	N.A.	60	20 h	[14]
Co_3O_4 nanofibers	0.1 M $TBAPF_6$ in ACN + 1%$_{vol}$ H_2O	-1.5 V vs NHE	65	27	8 h	This work

electrode preparation techniques.

In general, transition metal oxides such as Co_3O_4 are suitable for widespread use in heterogeneous catalysis due to their redox reactivity properties [15]. It is a p-type semiconductor with already known application areas of high-temperature solar selective absorbers, catalyst in the hydrocracking processes for fuel productions, as well as pigment for glasses and ceramics. The thermodynamic stability of the Co^{2+}/Co^{3+} oxidation states allows the variation in oxidizing or reducing states at ambient conditions. Compared to the structurally simplest rock salt monoxide (CoO), the spinel oxide Co_3O_4 offers high thermodynamic inertness at ambient temperature and at ambient oxygen partial pressure. In order to investigate the electrocatalytic properties of the nanofibrous Co_3O_4 we use a versatile electrospinning technique, which facilitates a low-cost processing [16,17]. For the electrochemical setup we prefer non-aqueous solutions such as acetonitrile in order to increase the solubility of CO_2 (0.27 mol/l at ambient pressure & temperature). The applicable electrochemical window for Co_3O_4 spans from $+2200$ mV to -1760 mV vs. NHE, which allows a detailed elucidation of Co_3O_4 nanofiber catalytic activity [18,19]. Since the product pathway in CO_2 reduction depends on the reaction medium, namely the electrolyte solution, small amount of water (1%$_{vol}$ H_2O, 0.55 mol L^{-1}) is added to acetonitrile in order to monitor the formate production as another important by-product in addition to CO formation, considering that Co_3O_4 favors formate generation in aqueous solution [14]. In terms of reaction control, we pursue a closed electrochemical system, in which we produce O_2 at the anode, while we observe reasonable yields of CO and formate at the cathode compartment [20]. Further, the addition of water has also the advantage to suppress the carbonate precipitation in organic, aprotic solvents and thus prevents any current and therefore any efficiency losses [20,21]. In the absence of water, only CO is observed as the main product with almost the same efficiency, but a corresponding loss in current. Moreover, the overpotential for CO evolution is calculated as 910 mV vs NHE for CO as referred to the standard potential of the CO_2/CO couple ($E°_{CO2/CO} = -650$ mV vs NHE) [22]. Electrochemical studies in an electrolyte solution of low proton availability reveal high yield in CO_2 reduction to CO (65%) and formate (27%) with Co_3O_4 nanofiber electrodes supported by the reaction medium. The notable performance of the nanofibrous Co_3O_4 is ascribed to the ease of the electrode preparation by electrospinning. This single-step technique enables the nano-structuring and thus gains an increased number of the catalytically active sites introduced by the fiber character. The nanocrystalline shaping of the oxide material to a nanofiber network allows us to enlarge the catalytically active surface per volume ratio, which is essential to obtain high yields in Faradaic efficiency. Nanofiber electrodes demonstrate an electrode stability of 8 h and an overall Faradaic efficiency of ~90% (for both CO and formate).

This suggests that even without the necessity of expensive and rare earth metals, in particular palladium, platinum, and many others [12] pristine nanofibrous Co_3O_4 can catalyze the CO_2 reduction towards CO mainly, assisted only by the reaction medium.
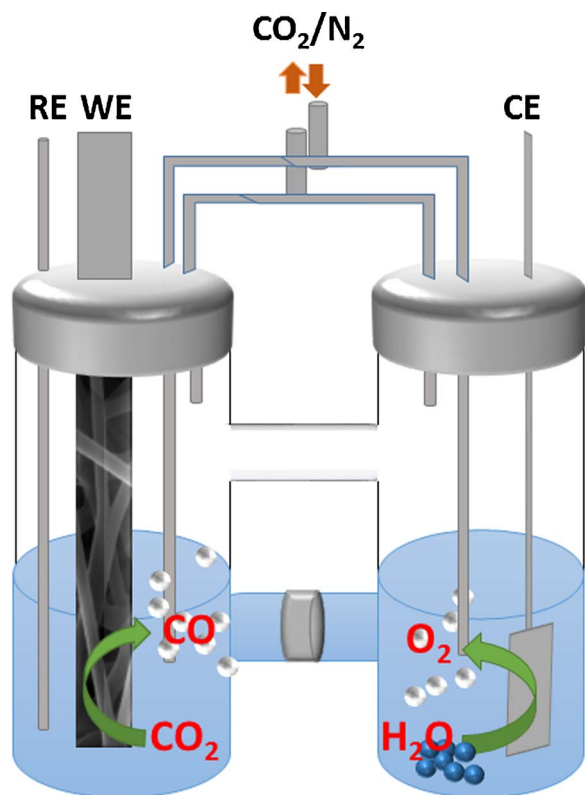
2. Experimental

2.1. Materials

The chemicals used in the present study include cobalt (II) chloride hexahydrate ($Cl_2Co.6H_2O$, 99%, Merck), dimethylformamide (DMF, 99%, Sigma-Aldrich), polyacrylontrile (PAN, Mw = 150,000, Sigma-Aldrich), acetonitrile (CH_3CN, 99.9%, Roth, 1%$_{vol}$ H_2O, 0.55 mol L^{-1}) and tetrabutylammoniumhexafluorophosphate (($CH_3CH_2CH_2CH_2$)$_4$N (PF$_6$), 99.00%, Fluka).

2.2. Methods

The electrospinning process for the Co_3O_4 nanofibers was achieved by using brand DC power supply and Kd Scientific brand syringe pump (New Era Pump System Inc.). The syringe is fixed in front of the collector at optimum conditions for electrospinning. The XRD pattern for the Co_3O_4 nanofibers was tested in powder mode using a Bruker Advance D8 XRD instrument, equipped with Cu Kα source ($\lambda = 1.5406$), while SEM (EVO LS 10, ZEISS, England) and Energy Dispersive X-ray spectrometer (Bruker 123 eV, Germany) were applied to analyze the morphology and elemental composition of Co_3O_4 nanofibers. The Raman study was conducted with Renishaw inVia, using a 532 nm laser. The thermogravimetric analysis (TGA) was performed with TGA/DSC 2 STAR^e System between 25 °C and 550 °C in air atmosphere at a scan rate of 5 °C/min. The optical properties of the obtained nanofibrous Co_3O_4 were analyzed on Biochrom Libra S22 UV–vis spectrometer in 400–1200 nm wavelength range [23]. Electrochemical experiments were performed using a JAISSLE Potentiostat Galvanostat IMP 88 PC and the amount of CO was analyzed with TRACE™ Ultra Gas Chromatograph equipped with a thermal conductivity detector (TCD) [3,20]. The electrochemical experiments were performed in the glovebox atmosphere. Furthermore, the CO_2 was delivered to the glovebox via a plastic tube from a gas cylinder which contains 99.995% pure CO_2. The compartments of the H-cell, as shown in Scheme 1, were purged with N_2 and CO_2 for 30 min, respectively, to have a complete saturation of the system and to prevent possible electrolyte exchange between the compartments, leading to a change in the CO_2 concentration of the environment. For the analysis of the CO gas, 2 mL samples were taken from the headspace with a gas-tight syringe and injected manually to the Thermo Scientific Trace GC Ultra gas chromatography. Helium was used as the carrier gas with a flow rate of 20 mL min^{-1}. The thermal conductivity detector (TCD) was kept at 200 °C. Capillary ion chromatography (CAP-IC) (Dionex ICS 5000, conductivity detector, AG19, CAP, 0.4 × 50 mm pre-column, AS19, CAP, 0.4 × 250 mm main column) with potassium hydroxide (KOH) as eluent for isocratic chromatography was justified for the analysis of liquid samples from the electrolyte solution before and after constant potential electrolysis. In CAP-IC the focus for product formation resulting from the CO_2 reduction was given to formate mainly due to low proton availability in the electrolyte solution. Samples were diluted 1:20 with highly purified 18 MΩ water for the injection. Injection was

Scheme 1. Experimental setup for electrochemical studies during CO_2 and N_2 purging in a standard three-electrode arrangement in H-Cell with gas inlet and outlet. Nanofibrous Co_3O_4 acts as a WE, Pt as a CE and Ag/AgCl as a QRE in a 0.1 M TBAPF$_6$ in acetonitrile with 1 vol% H_2O.

carried out by injecting 1ml of diluted sample with a syringe. The thickness of the nanofiber electrodes was measured with Bruker Dek-takXT.

2.3. Fabrication of the Co_3O_4 nanofiber

The solution of 2 mmol cobalt (II) chloride was prepared in 12 mL DMF and was stirred for 60 min to attain homogenous solution. Subsequent addition of 0.720 g of PAN (6% w/v) into the resulting solution at 60 °C was carried with continuous stirring for 48h in order to make slurry appropriate for electrospinning. Later on the velocity of the resulting homogenous solution was adjusted by the syringe pump at a feed rate of 0.3 mL/h. The applied voltage was 15 kV. Consequently, composite nanofibers from PAN/Cl$_2$Co.6H$_2$O were started to deposit on the FTO (Fluorine doped Tin Oxide) (6 × 0.8 cm^2) grounded square plates. Finally, the crystalline Co_3O_4 nanofibers were obtained by annealing at 550 °C for 30 min in air. The release of water molecule from the precursor (between 80 °C–220 °C) and the removal of the template polymer were followed by thermogravimetric analysis (TGA). PAN is decomposed after 450 °C into various kinds of gaseous vapors thereby leaving the nanofiber structure (see ESI, Fig. S1) [24,25].

2.4. Electrochemistry

In order to evaluate pristine Co_3O_4 nanofibers electrospun on FTO electrodes, electrochemical studies were conducted. Therefore, a standard three-electrode arrangement in a H-cell configuration was used with Co_3O_4 nanofiber as the working electrode (WE), Pt as the counter electrode (CE) and Ag/AgCl as aquasi reference electrode (QRE), all dipped into a 0.1 M Tetrabutylammoniumhexafluorophosphate (TBAPF$_6$) in acetonitrile with 1% H_2O added. We insert acetonitrile-water as an electrolyte solution to avoid precipitation of carbonate and

to prevent unwanted side-reactions in the anode space. The complete electrochemical system releases O_2 at the anode and primarily CO and formate at the cathode compartment. As shown in Scheme 1, the WE and QRE were placed in the same compartment of the H-cell, whereas the CE is in the second zone to avoid any back oxidation at the counter electrode. The anode and cathode compartments were separated by a glass frit of porosity nr.2 purchased from Labkon as the membrane between the cells. The Ag/AgCl quasi reference electrode was calibrated against ferrocene/ferrocenium (Fc/Fc$^+$) as an internal reference. The half-wave potential $E_{1/2}$ for Fc/Fc$^+$ was found at 400 mV vs. QRE. The head space volume in the cell was kept constant. Before starting each experiment the cell was flushed with N_2 and then CO_2 for 30 min, respectively. The scheme of the used electrochemical setup is shown in Scheme 1 [26].

3. Results and discussion

Before starting the electrochemical studies on the nanofibrous Co_3O_4 in order to test the catalytic activity, the optical, structural and elemental properties of the synthesized material were investigated by SEM, TEM, UV–vis, XRD, EDX, TGA and RAMAN techniques, respectively. In Fig. 1 the SEM images of Co_3O_4 nanofibers are shown before annealing (a and b), after annealing at 550 °C (c and d) as well as after the electrochemical studies in 0.1 M TBAPF$_6$ in acetonitrile-water electrolyte solution (e and f).

From the SEM images it is clearly observed that miniscule changes on the nanofiber structure of Co_3O_4 are found, although high temperature annealing and exhaustive electrolysis are applied to the material. After the annealing process (1c and d) the diameter of the Co_3O_4 nanofiber was shrinking from 220 nm to 170 nm, due to various kinds of gaseous organic compounds, i.e. the template polymer Polyacrylnitrile (PAN) and water vapors leaving the nanofiber [27]. Further the TEM images of the nanofibrous material are taken as shown in Fig. 2a, indicating very smooth and uniform surface of the nanofibers. Moreover, the selected area diffraction (SAED) pattern of the nanofibers is presented in Fig. 2b which matches with the structure of cubic Co_3O_4 (S.G:Fd-3 m) and demonstrates that fibers have a single crystalline nature. Further, the energy dispersive X-ray (EDX) elemental maps for the Co and O atoms are illustrated in Fig. 2c–e. The elemental mapping images reveal that Co and O are homogeneously distributed throughout the fiber.

Fig. 3a presents the UV–vis spectrum of Co_3O_4 nanofiber. The prominent absorption from Co_3O_4 nanofibers in the range of 400 nm to 1200 nm are recorded. Two peaks at 450 nm and 672 nm are observed corresponding to the band structure of Co_3O_4 with O (II) to Co (II) and O (II) to Co (III) charge transfer transition, respectively. The optical band gap is determined by using the Tauc equation which can be expressed as $\alpha h\upsilon = k\ (h\upsilon - E_g)^n$, where E_g describes the band gap, $h\upsilon$ is the photon energy, k is the constant, α is the absorption coefficient and n is a value that depends on the nature of the transition [28,29]. In the present case of Co_3O_4, n is set as ½ for direct allowed transition. Thus, by plotting $(\alpha h\upsilon)^2$ against $h\upsilon$, the band gap can be extracted [17,30]. Consistent with the literature, two transitions with energy gap values are estimated at 1.43 eV and 2.1 eV [16,31,32]. Further, a similar transition is extracted from the cyclic voltammogram of Co_3O_4 recorded in nitrogen atmosphere (see Fig. 4). From the calculated valence and conduction band, electrochemical transition with the following energy gap is determined as 1.4 eV [33]. The formula for the calculations of the band gap can be found in the supporting information.

The structural and elemental characterization were followed by XRD, EDX and RAMAN techniques, respectively, as shown in Fig. 3b–d. The XRD patterns of the Co_3O_4 nanofibers exhibit a cubic phase structure with the peak positions at 2θ = 19.06˚, 31.19˚, 36.68˚, 38.46˚, 44.81˚, 55.80˚, 59.35˚ and 65.18˚, in good agreement with JCPDS 00-043-1003. Consistent with standard Co_3O_4 XRD pattern these peaks are assigned to (111), (220), (311), (222), (400), (422), (511), and (440)
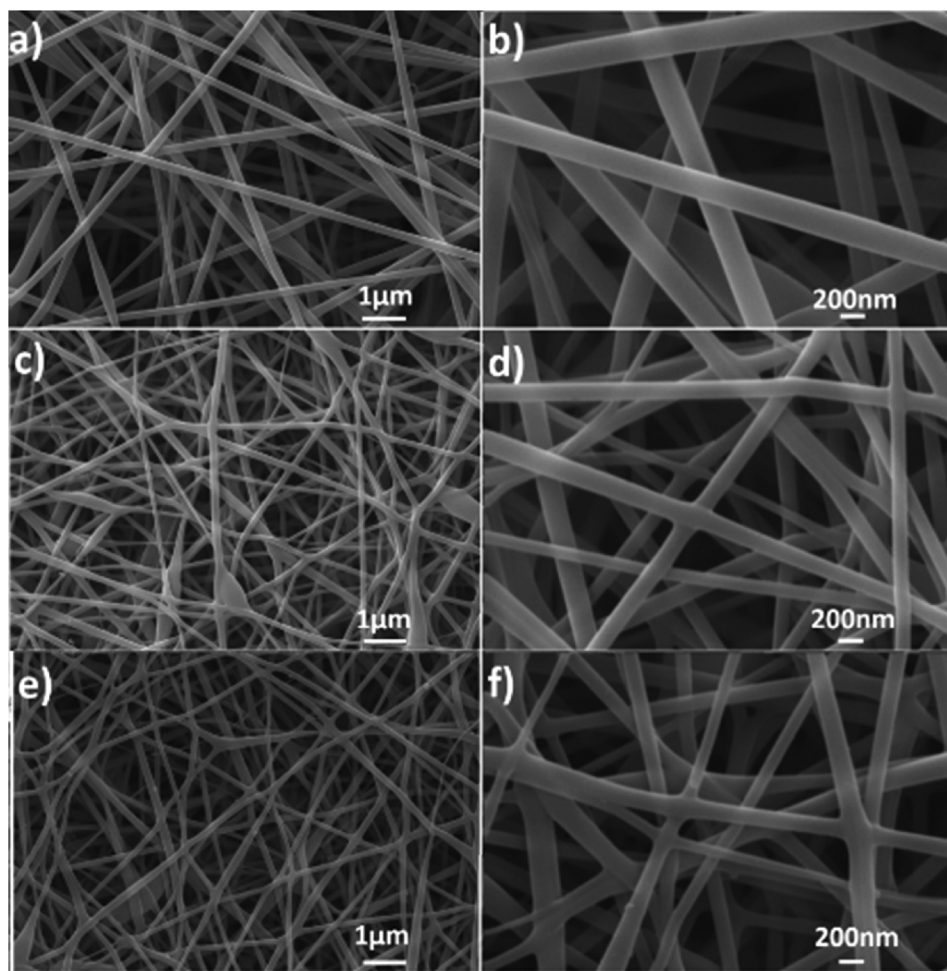
Fig. 1. SEM images of Co-PAN nanofibers before annealing (a and b); after annealing at 550 °C for 30 min in air (c and d); and after electrochemical investigations (e and f).

diffraction lines of cubic crystalline phase [16,34–36]. Additionally, in Fig. 3b, the XRD pattern of the starting material cobalt (II) chloride with the template polymer (PAN) is shown (red), demonstrating the formation of Co_3O_4 upon annealing process in air for 30 min (blue).

The Energy Dispersive X-Ray (EDX) spectrum of Co_3O_4 nanofiber is provided in the Fig. 3c. The chemical composition of the prepared Co_3O_4 nanofiber is in good agreement with the theoretical values as it is evident from the EDX results. In order to test any degradation of the nanofibrous transition metal oxide, all of the analytical experiments (XRD and EDX) as well as the electrochemical investigations after the electrolysis were conducted conscientiously (see ESI, Figs. S2 and S3) indicating no significant differences or degradation of the nanofibrous material.

The Raman spectrum of the Co_3O_4 nanofiber is visualized in Fig. 3d. In the recorded range of the spectrum, five bands are observed, located at 190, 470, 516, 608 and 678 cm^{-1} corresponding to the F_{2g}, E_g, F_{2g}, F_{2g}, and A_{1g} Raman active modes, respectively, in agreement with the crystalline phase of Co_3O_4 as reported in the literature [37–39].

Once the composition of the nanofibrous material was identified as Co_3O_4 by analytical techniques, electrochemical studies were conducted to test the catalytic activity of the pristine cobalt oxide towards CO_2 reduction to CO without using any metal additives, such as platinum, palladium or potassium, as previously applied [12]. Thus the electrode fabrication was followed as described in the experimental section. The electrochemical experiment was conducted in a H-cell configuration in order to avoid the reoxidation on the counter electrode. The cyclic voltammetry (CV) scans of Co_3O_4 nanofibrous electrode over 40 cycles, as well as the CV as a function of the scan rate are

shown in the supporting information (see ESI, Figs. S4 and S5).

Fig. 4a shows the cyclic voltammetry responses of the FTO electrodes without Co_3O_4 nanofibers (green and brown) in comparison with Co_3O_4 nanofibers on FTO electrodes (blue and red). From the control experiment of pristine FTO electrodes, it is clearly seen that there is a negligible change in current of the FTO electrode after N_2 and CO_2 purging whereas an enhancement in current is obtained with Co_3O_4 nanofibers on the FTO electrodes. Thus, the reductive current indicates the catalytic activity of Co_3O_4 nanofibers in a sense of reducing CO_2. As direct proof for the advancements by nanofibers we have included bulk Co_3O_4 electrodes (prepared by dropcasting) in parallel to the electrospun fibers. We denote that material synthesis remains the same with only the electrode preparation changed. As such, we compare the electrodes under N_2 and CO_2 atmosphere (see ESI, Fig. S6). As expected, (with and without CO_2) the nanofiber electrodes have superior performance (i.e. under CO_2 atmosphere the reductive currents are enhanced a factor of 4 by nanofiber electrodes) shown in Fig. 4b. Thus, we attribute the remarkable performance of the Co_3O_4 nanofibers to the higher effective surface area introduced by the fiber character. In Fig. 5, an outline about the electrochemical attitude towards the reduction of CO_2 by nanofibrous Co_3O_4 as an electrocatalyst is presented. In this study, the Co_3O_4 nanofiber electrodes were examined in the electroreduction of CO_2 to CO and formate. As shown in Fig. 5a, an increased amount of formed products is observed by an increased electrolysis time. After a while CO formation dominates over formate, due to the small amount of proton existence in the electrolyte solution. This insinuates that the selectivity of product formation can be conducted by the electrolyte solution composition [40]. The optimum parameter for
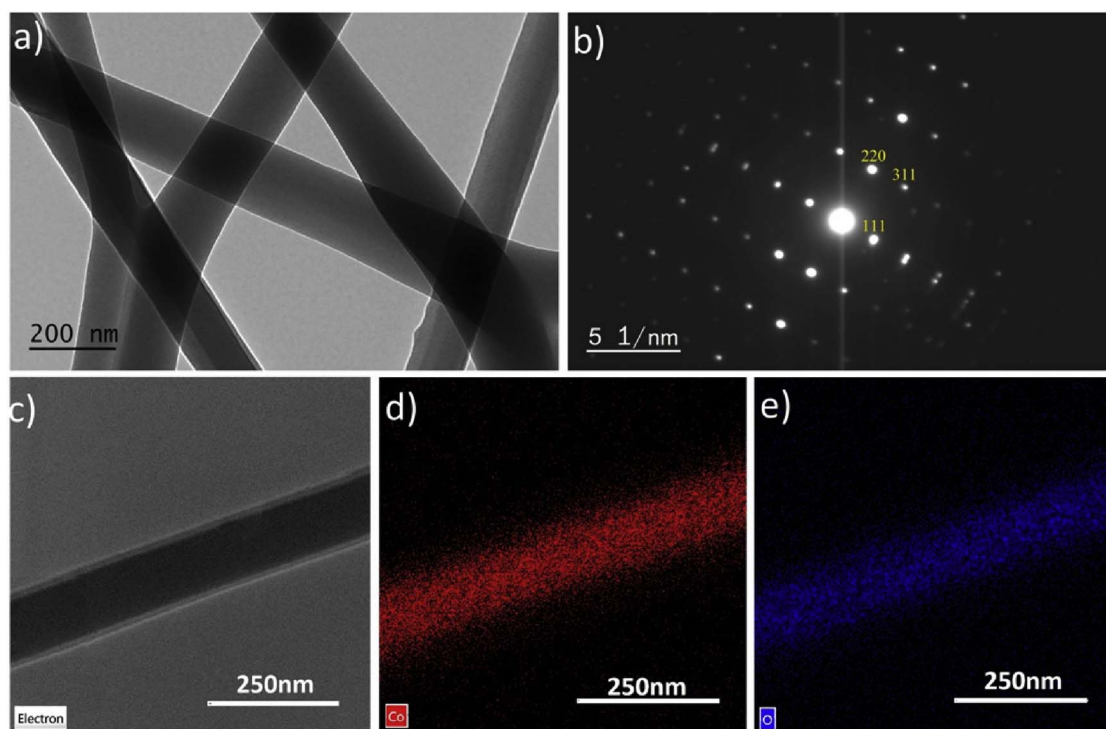
Fig. 2. (a) TEM images taken of Co_3O_4 nanofibers, (b) selected area diffraction (SAED) of Co_3O_4 (c–e) Elemental mapping of the nanofibrous Co_3O_4 homogenously distributed on the electrode surface.
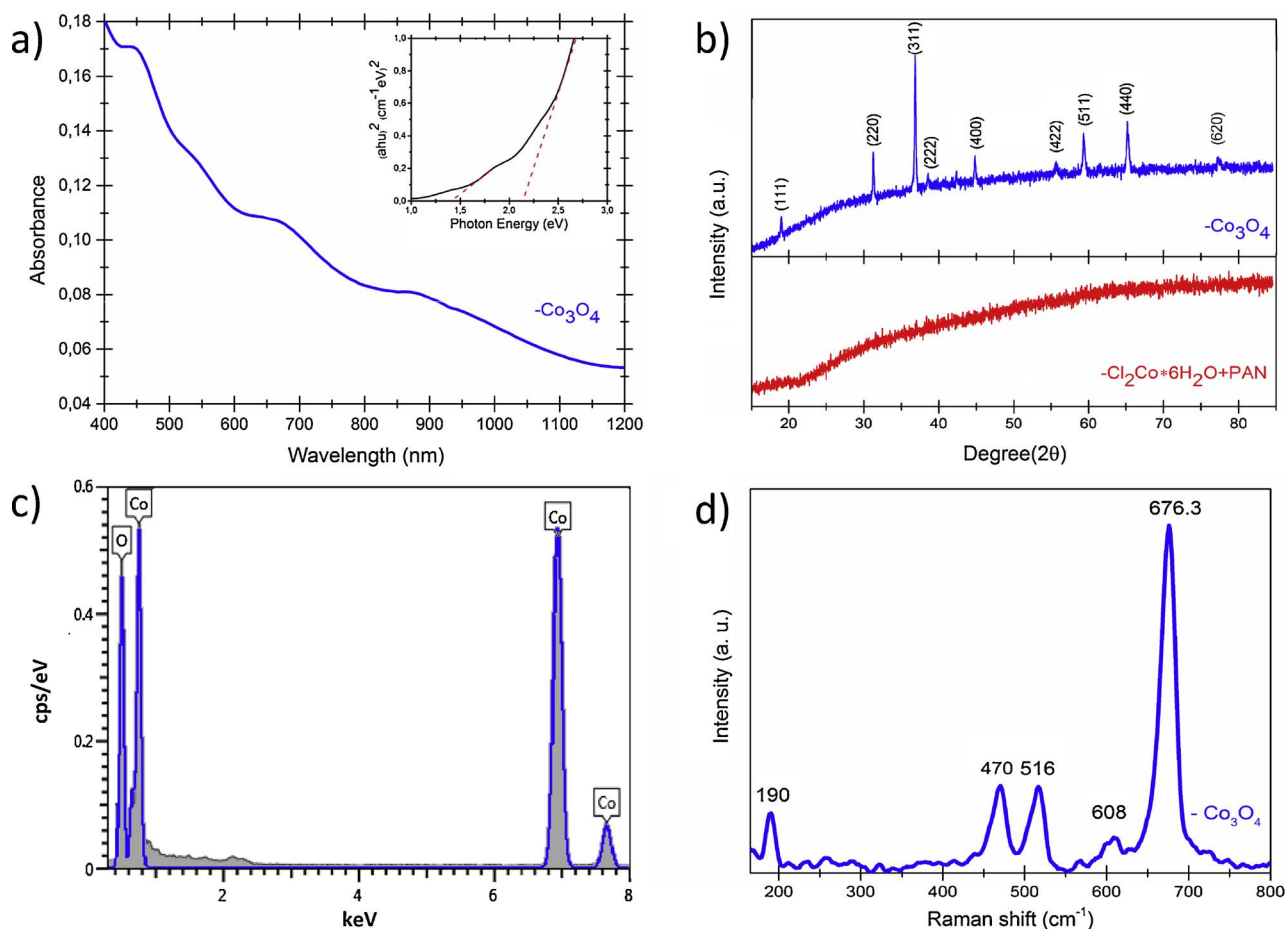

Fig. 3. (a) UV–vis spectrum of Co_3O_4 nanofibers, (b) XRD-pattern of Co_3O_4 nanofiber (blue) in comparison to the starting material together with the polymer template (red), (c) Energy Dispersive X-Ray (EDX) Spectrum of Co_3O_4 nanofiber, (d) RamanSpectrum of Co_3O_4 nanofiber sintered at 550 °C. (For interpretation of the references to colour in this figure legend, the reader is referred to the web version of this article.)
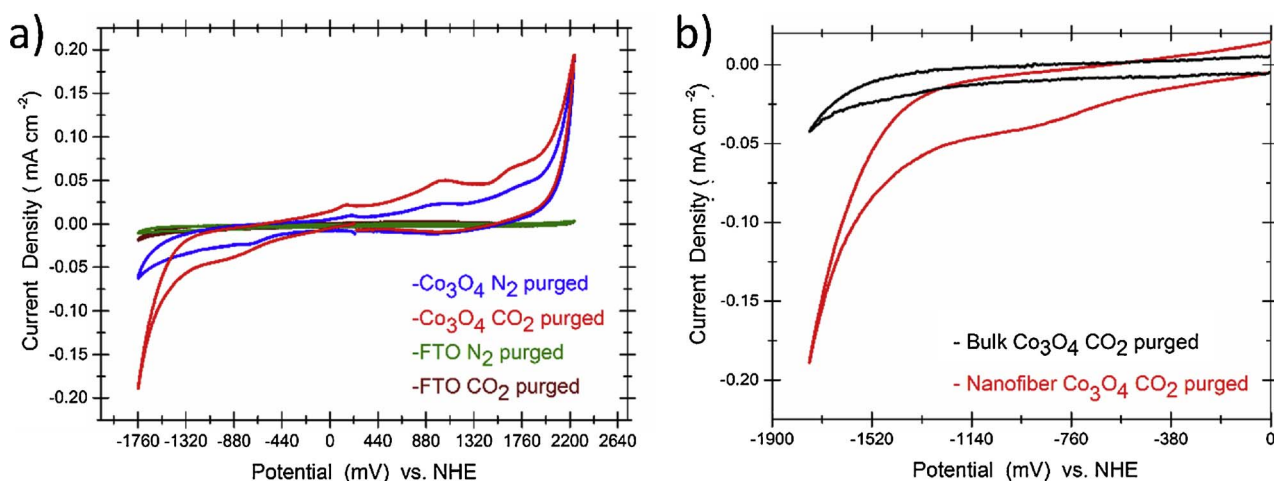
Fig. 4. (a) Cyclic voltammogramms of FTO electrodes (green and brown) and Co_3O_4 nanofibers deposited onto FTO electrodes (blue and red) purged with N_2 and CO_2 for 30 min at a scan rate 30 mV s^{-1}, (b) comparison of bulk and nanofiber electrode performance for CO_2RR using Co_3O_4 electrocatalyst. Enhancement in reductive current is obtained only in the presence nanofibrous Co_3O_4 purged with CO_2 (red). (For interpretation of the references to colour in this figure legend, the reader is referred to the web version of this article.)

the operating voltage, at which the electrolysis should be carried out, is demonstrated in Fig. 5b in which the highest faradaic efficiency was attained at −1560 mV vs NHE for CO production. The

chronoamperometry result at a constant electrolysis potential of −1560 mV vs NHE is exhibited in Fig. 5c. Hence, it is clearly evident that the nanofibrous Co_3O_4 electrodes remain working for 8 h at a
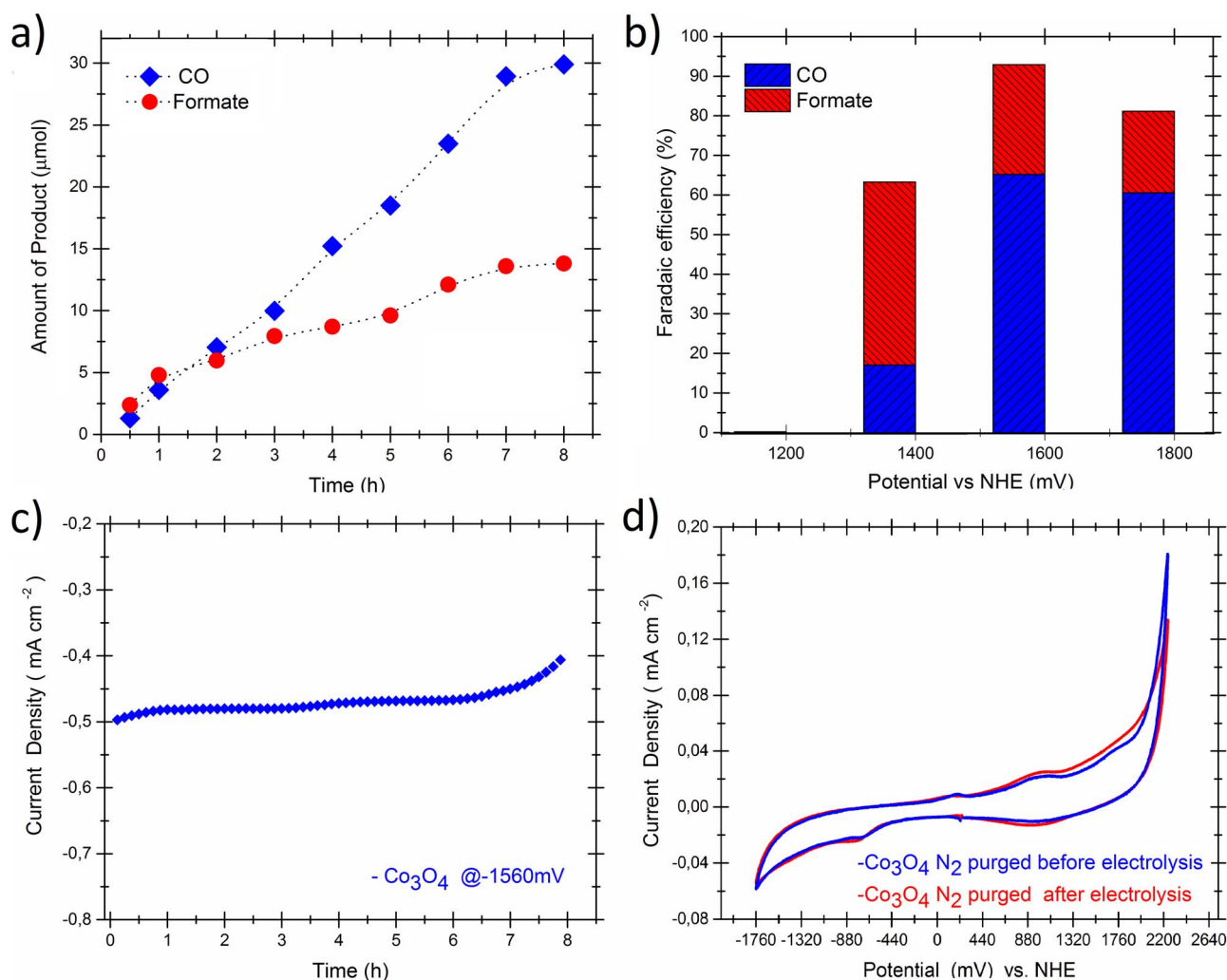

Fig. 5. Study of the electroreduction of CO_2 using nanofibrous Co_3O_4, (a) increasing amount of produced CO gas and formate as a function of time at a constant electrolysis potential of −1560 mV vs NHE, (b) examination of electrolysis voltage versus faradaic efficiency, (c) chronoamperometry results, (d) Cyclic voltammograms of the nanofiber electrode recorded before and after electrolysis at a scan rate of 30 mV s^{-1}.

stable current density of nearly 0.5 mA/cm^2 based on the geometrical area of the electrode. Only after 7 h of operation at a constant potential, a slight saturation of the electrode performance is recorded, probably due to the discontinuity of the electrolyte system. In addition, Fig. 5d presents the cyclic voltammograms of the Co$_3$O$_4$ electrode measured before and after the electrolysis for 8 h, indicating insignificant degradation of the nanofiber electrodes, still stable and operational after exhaustive conditions. The gas chromatograms at different electrolysis times, can be found in the supporting information (see ESI, Fig. S7).

The electrocatalytic performance for the CO$_2$ reduction of the Co$_3$O$_4$ nanofiber electrodes was determined by faradaic efficieny according to the Eq. (1).

$$\eta = \frac{2*(\text{amount of CO in the gas phase} + \text{amount of CO in solution})}{\text{number of electrons}} \quad (1)$$

The amount of CO in the gas phase was detected by GC analysis and the amount of CO in solution was estimated by using the Henry's law (2).
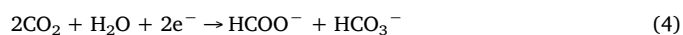
$$p = k_H * c \quad (2)$$

In which p is the partial pressure of CO above the solution, c the concentration of CO in solution and k_H the Henry constant (2507 atm mol$_{solvent}$ mol$_{CO}$) [41]. The number of electrons put into the system during CO$_2$ electrolysis was determined by integration of the I/t curve over time of experiment.

Taking these considerations into account, a Faradaic efficiency for the CO$_2$ reduction to CO was found to be 65% with Co$_3$O$_4$ nanofiber electrodes. With 27% Faradaic efficiency formate is produced as a by-product, due to some proton coexistence in the electrolyte solution. No other side products were detected by the applied analytical GC and CAP-IC techniques. The capillary ion chromatography results for the formate production are provided in the supporting information (see ESI, Fig. S8). The control experiment with only FTO electrodes at the same electrolysis conditions did not give detectable amounts of CO as a result [3,42]. Furthermore, bulk electrolysis with FTO/ Co$_3$O$_4$ electrodes under N$_2$ saturation was performed as well, which lead to no measureable CO amount in the GC analysis (see ESI, Fig. S9).

Based on the literature, in Scheme 2 the proposed reaction pathway of the CO$_2$ reduction with Co$_3$O$_4$ nanofibers is illustrated. Mechanistic insights for CO$_2$RR on Co-based electrocatalysts have been discussed for water-based systems [13]. CO$_2$RR reduction mechanism is determined by the initial electron transfer reaction i.e. CO$_2$ activation to CO$_2$$^{*-}$ and subsequent rate determining steps assisted by H$^+$. The product distribution relies on competing pathways leading to the various products (formate, CO or oxalate) in transition-metal chalcogenides and depends preponderantly on the H$^+$ concentration (i.e. in water, the product is mainly formate, while in non-aqueous, but still H$^+$-containing electrolyte systems (ionic liquids-water and acetonitrile-water) CO is

dominant). The self-coupling of CO$_2$$^{*-}$ plays a subordinate role (negligible pathway for the formation of oxalate).In this particular case, it is presumed that CO$_2$ is first adsorbed on catalytically active Co$_3$O$_4$ nanofibers. Next, the adsorbed CO$_2$ gains one electron from the nanofibrous electrode and is converted to CO$_2$$^{*-}$ at negative cathode potentials. Subsequently, due to the oxygen-carbon coupling of CO$_2$$^{*-}$ with CO$_2$ in the organic electrolyte system, the evolution of CO is observed, consistent with literature [21]. Moreover, the low amount of water available in the electrolyte, causes the protonation of CO$_2$$^{*-}$ followed by an electron transfer in the solution leads to the formation of formate [13,21,43]. The overall reactions are summarized as the following:

$$CO_2 + 2\ H^+ + 2\ e^- \rightarrow CO + H_2O \quad (3)$$

$$2CO_2 + H_2O + 2e^- \rightarrow HCOO^- + HCO_3^- \quad (4)$$

Although in low proton media, the competing reactions are the oxalate formation by the self-coupling of the CO$_2$$^{*-}$ anions, carbon monoxide and formate production, the formation of oxalate is not observed after electrolysis using Co$_3$O$_4$ nanofibers and further the precipitation of carbonate is suppressed by the presence of water. In this particular case of nanofibrous Co$_3$O$_4$ electrodes, the electrochemical reduction of CO$_2$ yield in 65% Faradaic efficiency of CO production and 27% Faradaic efficiency of formate. We attribute the high yield of CO formation mainly to the polar, aprotic electrolyte solution acetonitrile. As previously mentioned, in the absence of water, only CO is observed as the main product, but a corresponding loss in current. Hence, we believe that the formate production is due to the consumption of the little proton amount in the supporting electrolyte and is therefore considered as a valuable by-product. These results display that the product selectivity in CO$_2$ reduction can be influenced by the choise of electrolyte media. Since no further side products other than CO and formate were detected by the analytical methods, the remaining ~8% of the current is suggested to be consumed by the decomposition and/or heating process of the material [14,21,44]. Accordingly, the overpotential of the electrochemical system is determined as 910 mV vs NHE as referred to the standard potential of the CO$_2$/CO couple (E°$_{CO2/CO}$ = −650 mV vs NHE) in acetonitrile-water electrolyte [22,45].

Although high current density and low overpotential are desired in catalytic processes, the overpotential of the Co$_3$O$_4$ nanofiber electrodes seems to be comparable with those of inorganic catalysts, namely metals such as copper, silver and gold [46].Thus, the cobalt oxide electrodes indeed reduce CO$_2$ electrocatalytically due to the nanofibrous nature of the active material and hence the increased amount of catalytically active sites. A stable operation of the electrodes in a acetonitrile-water electrolyte for many hours at moderate operation voltage and high yields in CO$_2$ conversion make the Co$_3$O$_4$ nanofibers applicable in heterogeneous electrocatalysis.

4. Conclusion

In this study we report the main production of CO from CO$_2$ using Co$_3$O$_4$ nanofiber electrodes without any other metal additives with a Faradaic efficiency of 65%. The residual by-product formation towards formate (27%) is monitored by means of the electrolyte solution composition. The heterogenous catalysis with cobalt oxide was achieved through the deposition of the catalytic active material by using the electrospinning technique with a simple synthesis procedure. The obtained nanofiber electrodes were firstly investigated by UV–vis, SEM, TEM, TGA, Raman, XRD and EDX techniques in order to find out the optical, elemental and structural properties. Later, an extended study on Co$_3$O$_4$ nanofibers electrochemical behavior was conducted, describing the electrocatalytic activity of the pristine cobalt oxide without any metal supplement, i.e palladium, platinum, etc. Additionally, the analysis after exhaustive electrolysis showed that the nanofibers are stable under operating conditions. It is remarkable that the catalytic active material cobalt oxide reduces CO$_2$ to CO primarily with such a
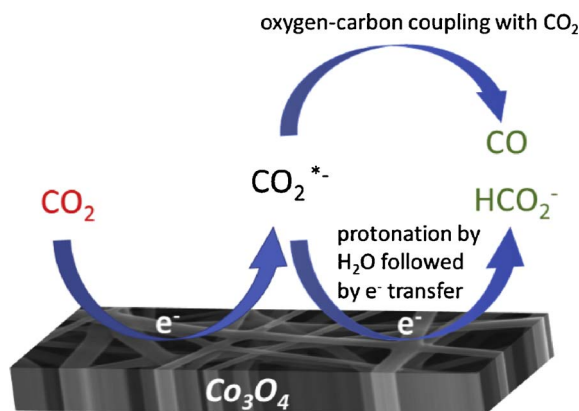
Scheme 2. Proposed reaction mechanism of CO$_2$ reduction using Co$_3$O$_4$ nanofiber electrodes in a low proton electrolyte solution.

high Faradaic efficiency without the necessity of expensive and rare metals at ordinary potentials and electrode stability times. Since, CO itself is another important feedstock for many other chemical and fuel productions, we believe reducing CO_2 to CO with these nanofiber electrodes of pristine Co_3O_4, without further metal additives, are employable for future large scale applications due to economic and time saving production of the catalytic active material.

Acknowledgements

Appendix A. Supplementary data

Supplementary material related to this article can be found, in the online version, at doi:https://doi.org/10.1016/j.apcatb.2018.02.017.

References

[1] J.P. O'Byrne, R.E. Owen, D.R. Minett, S.I. Pascu, P.K. Plucinski, M.D. Jones, D. Mattia, High CO_2 and CO conversion to hydrocarbons using bridged Fe nanoparticles on carbon nanotubes, Catal. Sci. Technol. 3 (2013) 1202–1207.
[2] H.A. Schwarz, R.W. Dodson, Reduction potentials of Co2- and the alcohol radicals, J. Phys. Chem.-US 93 (1989) 409–414.
[3] E. Portenkirchner, J. Gasiorowski, K. Oppelt, S. Schlager, C. Schwarzinger, H. Neugebauer, G. Knor, N.S. Sariciftci, Electrocatalytic reduction of carbon dioxide to carbon monoxide by a polymerized film of an alkynyl-substituted rhenium(I) complex, Chemcatchem 5 (2013) 1790–1796.
[4] H.R. Jhong, S.C. Ma, P.J.A. Kenis, Electrochemical conversion of CO_2 to useful chemicals: current status, remaining challenges, and future opportunities, Curr. Opin. Chem. Eng. 2 (2013) 191–199.
[5] S. Kaneco, M. Yabuuchi, H. Katsumata, T. Suzuki, K. Ohta, Electrochemical reduction of CO_2 to methane in methanol at low temperature, Abstr. Pap. Am. Chem. Soc. 223 (2002) U573.
[6] J. Ronge, T. Bosserez, D. Martel, C. Nervi, L. Boarino, F. Taulelle, G. Decher, S. Bordiga, J.A. Martens, Monolithic cells for solar fuels, Chem. Soc. Rev. 43 (2014) 7963–7981.
[7] W.W. Russell, G.H. Miller, Catalytic hydrogenation of carbon dioxide to higher hydrocarbons1, J. Am. Chem. Soc. 72 (1950) 2446–2454.
[8] S. Singh, R.K. Gautam, K. Malik, A. Verma, Ag-Co bimetallic catalyst for electrochemical reduction of CO_2 to value added products, J. CO_2 Util. 18 (2017) 139–146.
[9] S. Roy, B. Sharma, J. Pécaut, P. Simon, M. Fontecave, P.D. Tran, E. Derat, V. Artero, Molecular cobalt complexes with pendant amines for selective electrocatalytic reduction of carbon dioxide to formic acid, J. Am. Chem. Soc. 139 (2017) 3685–3696.
[10] S. Gao, Z. Sun, W. Liu, X. Jiao, X. Zu, Q. Hu, Y. Sun, T. Yao, W. Zhang, S. Wei, Y. Xie, Atomic layer confined vacancies for atomic-level insights into carbon dioxide electroreduction, Nat. Commun. 8 (2017) 14503.
[11] J. Shen, R. Kortlever, R. Kas, Y.Y. Birdja, O. Diaz-Morales, Y. Kwon, I. Ledezma-Yanez, K.J.P. Schouten, G. Mul, M.T.M. Koper, Electrocatalytic reduction of carbon dioxide to carbon monoxide and methane at an immobilized cobalt protoporphyrin, Nat. Commun. 6 (2015) 8177.
[12] R.E. Owen, J.P. O'Byrne, D. Mattia, P. Plucinski, S.I. Pascu, M.D. Jones, Cobalt catalysts for the conversion of CO_2 to light hydrocarbons at atmospheric pressure, Chem. Commun. 49 (2013) 11683–11685.
[13] S. Gao, Y. Lin, X. Jiao, Y. Sun, Q. Luo, W. Zhang, D. Li, J. Yang, Y. Xie, Partially oxidized atomic cobalt layers for carbon dioxide electroreduction to liquid fuel, Nature 529 (2016) 68–71.
[14] S. Gao, X. Jiao, Z. Sun, W. Zhang, Y. Sun, C. Wang, Q. Hu, X. Zu, F. Yang, S. Yang, L. Liang, J. Wu, Y. Xie, Ultrathin Co_3O_4 layers realizing optimized CO_2 electroreduction to formate, Angew. Chem. Int. Ed. 55 (2016) 698–702.
[15] A. Zecchina, D. Scarano, S. Bordiga, G. Spoto, C. Lamberti, Surface structures of oxides and halides and their relationships to catalytic properties, Adv. Catal. 46 (2001) 265–397.
[16] P.S. Patil, L.D. Kadam, C.D. Lokhande, Preparation and characterization of spray pyrolysed cobalt oxide thin films, Thin Solid Films 272 (1996) 29–32.
[17] S.C. Petitto, E.M. Marsh, G.A. Carson, M.A. Langell, Cobalt oxide surface chemistry: the interaction of CoO(100), Co_3O_4(110) and Co_3O_4(111) with oxygen and water, J. Mol. Catal. A-Chem. 281 (2008) 49–58.
[18] C. Cadena, J.L. Anthony, J.K. Shah, T.I. Morrow, J.F. Brennecke, E.J. Maginn, Why is CO_2 so soluble in imidazolium-based ionic liquids? J. Am. Chem. Soc. 126 (2004) 5300–5308.

[19] A. Gennaro, A.A. Isse, E. Vianello, Solubility and electrochemical determination of co2 in some dipolar aprotic-solvents, J. Electroanal. Chem. 289 (1990) 203–215.
[20] H. Coskun, A. Aljabour, P. De Luna, D. Farka, T. Greunz, D. Stifter, M. Kus, X. Zheng, M. Liu, A.W. Hassel, W. Schöfberger, E.H. Sargent, N.S. Sariciftci, P. Stadler, Biofunctionalized conductive polymers enable efficient CO2 electroreduction, Sci. Adv. 3 (2017).
[21] C. Amatore, J.M. Saveant, Mechanism and kinetic characteristics of the electrochemical reduction of carbon-dioxide in media of low proton availability, J. Am. Chem. Soc. 103 (1981) 5021–5023.
[22] C. Costentin, S. Drouet, M. Robert, J.M. Saveant, A local proton source enhances CO2 electroreduction to CO by a molecular Fe catalyst, Science 338 (2012) 90–94.
[23] H. Shao, X. Zhao, Y. Wang, R. Mao, Y. Wang, M. Qiao, S. Zhao, Y. Zhu, Synergetic activation of peroxymonosulfate by Co3O4 modified g-C3N4 for enhanced degradation of diclofenac sodium under visible light irradiation, Appl. Catal. B: Environ. 218 (2017) 810–818.
[24] F. Ozel, Earth-abundant quaternary semiconductor Cu2MSnS4 (M = Fe, Co, Ni and Mn) nanofibers: fabrication, characterization and band gap arrangement, J. Alloy. Compd. 657 (2016) 157–162.
[25] F. Ozel, M. Kus, A. Yar, E. Arkan, M.Z. Yigit, A. Aljabour, S. Buyukcelebi, C. Tozlu, M. Ersoz, Electrospinning of Cu2ZnSnSe4-xSx nanofibers by using PAN as template, Mater. Lett. 140 (2015) 23–26.
[26] E. Portenkirchner, S. Schlager, D. Apaydin, K. Oppelt, M. Himmelsbach, D.A.M. Egbe, H. Neugebauer, G. Knor, T. Yoshida, N.S. Sariciftci, Using the alkynyl-substituted rhenium(I) complex (4,4'-bisphenyl-ethynyl-2,2'-bipyridyl)Re(CO)(3)Cl as catalyst for CO2 reduction-synthesis, Charact. Appl. Electrocatal. 6 (2015) 185–197.
[27] L. Fan, W. Zhang, S. Zhu, Y. Lu, Enhanced lithium storage capability in Li-ion batteries using porous 3D Co3O4 nanofiber anodes, Ind. Eng. Chem. Res. 56 (2017) 2046–2053.
[28] C.T. Ho, T.H. Weng, C.Y. Wang, S.J. Yen, T.R. Yew, Tunable band gaps of Co3-xCuxO4 nanorods with various Cu doping concentrations, RSC Adv. 4 (2014) 20053–20057.
[29] S. Kandula, P. Jeevanandam, A facile synthetic approach for SiO2@Co3O4 core-shell nanorattles with enhanced peroxidase-like activity, RSC Adv. 5 (2015) 5295–5306.
[30] F. Ozel, E. Aslan, B. Istanbullu, O. Akay, I.H. Patir, Photocatalytic hydrogen evolution based on Cu2ZnSnS4, Cu2NiSnS4 and Cu2CoSnS4 nanocrystals, Appl. Catal. B-Environ. 198 (2016) 67–73.
[31] J.S. Gwag, Y. Sohn, Interfacial natures and controlling morphology of Co oxide nanocrystal structures by adding spectator Ni ions, B Korean Chem. Soc. 33 (2012) 505–510.
[32] M. Long, W.M. Cai, J. Cai, B.X. Zhou, X.Y. Chai, Y.H. Wu, Efficient photocatalytic degradation of phenol over Co3O4/BiVO4 composite under visible light irradiation, J. Phys. Chem. B 110 (2006) 20211–20216.
[33] X.S. Zhu, J.F. Wang, D. Nguyen, J. Thomas, R.A. Norwood, N. Peyghambarian, Linear and nonlinear optical properties of Co3O4 nanoparticle-doped polyvinyl-alcohol thin films, Opt. Mater. Express 2 (2012) 103–110.
[34] M. Kumar, A. Subramania, K. Balakrishnan, Preparation of electrospun Co3O4 nanofibers as electrode material for high performance asymmetric supercapacitors, Electrochim. Acta 149 (2014) 152–158.
[35] H. Xu, J.X. Zhuang, Y. Chen, J.X. Wu, J.L. Zhang, Preparation and performance of Co3O4-NiO composite electrode material for supercapacitors, RSC Adv. 4 (2014) 15511–15517.
[36] X.G. Ye, X.G. Mang, H.Y. Mi, S.D. Yang, Hydrothermal microemulsion synthesis of Co3O4 with different morphologies and their electrochemical capacitance, Acta Phys.-Chim. Sin. 24 (2008) 1105–1110.
[37] Y. Ding, Y. Wang, L.A. Su, M. Bellagamba, H. Zhang, Y. Lei, Electrospun Co(3)O(4) nanofibers for sensitive and selective glucose detection, Biosens. Bioelectron. 26 (2010) 542–548.
[38] W.-H. Ryu, T.-H. Yoon, S.H. Song, S. Jeon, Y.-J. Park, I.-D. Kim, Bifunctional composite catalysts using Co3O4 nanofibers immobilized on nonoxidized graphene nanoflakes for high-capacity and long-cycle Li–O2 batteries, Nano Lett. 13 (2013) 4190–4197.
[39] S.L. Xiong, C.Z. Yuan, M.F. Zhang, B.J. Xi, Y.T. Qian, Controllable synthesis of mesoporous Co3O4 nanostructures with tunable morphology for application in supercapacitors, Chem.-Eur. J. 15 (2009) 5320–5326.
[40] S.B. Adler, Mechanism and kinetics of oxygen reduction on porous La1-xSrxCoO3-delta electrodes, Solid State Ion. 111 (1998) 125–134.
[41] Z.K. Lopez-Castillo, S.N.V.K. Aki, M.A. Stadtherr, J.F. Brennecke, Enhanced solubility of oxygen and carbon monoxide in CO2-expanded liquids, Ind. Eng. Chem. Res. 45 (2006) 5351–5360.
[42] A. Aljabour, D.H. Apaydin, H. Coskun, F. Ozel, M. Ersoz, P. Stadler, N.S. Sariciftci, M. Kus, Improvement of catalytic activity by nanofibrous CuInS2 for electrochemical CO2 reduction, ACS Appl. Mater. Interfaces 8 (2016) 31695–31701.
[43] M. Asadi, K. Kim, C. Liu, A.V. Addepalli, P. Abbasi, P. Yasaei, P. Phillips, A. Behranginia, J.M. Cerrato, R. Haasch, P. Zapol, B. Kumar, R.F. Klie, J. Abiade, L.A. Curtiss, A. Salehi-Khojin, Nanostructured transition metal dichalcogenide electrocatalysts for CO2 reduction in ionic liquid, Science 353 (2016) 467–470.
[44] S.C. Ma, Y.C. Lan, G.M.J. Perez, S. Moniri, P.J.A. Kenis, Silver supported on Titania as an active catalyst for electrochemical carbon dioxide reduction, Chemsuschem 7 (2014) 866–874.
[45] Y. Matsubara, D.C. Grills, Y. Kuwahara, Thermodynamic aspects of electrocatalytic CO2 reduction in acetonitrile and with an ionic liquid as solvent or electrolyte, ACS Catal. 5 (2015) 6440–6452.
[46] Y.-C. Hsieh, S.D. Senanayake, Y. Zhang, W. Xu, D.E. Polyansky, Effect of chloride anions on the synthesis and enhanced catalytic activity of silver nanocoral electrodes for CO2 electroreduction, ACS Catal. 5 (2015) 5349–5356.